Exploitation of an iron transporter for bacterial protein antibiotic import

Paul White[a], Amar Joshi[a,1], Patrice Rassam[a], Nicholas G. Housden[a], Renata Kaminska[a], Jonathan D. Goult[a], Christina Redfield[a], Laura C. McCaughey[a,b], Daniel Walker[c], Shabaz Mohammed[a], and Colin Kleanthous[a,2]

[a]Department of Biochemistry, University of Oxford, Oxford OX1 3QU, United Kingdom; [b]iThree Institute, University of Technology Sydney, Sydney, NSW 2007, Australia; and [c]Institute of Infection, Immunity & Inflammation, College of Medical, Veterinary & Life Sciences, University of Glasgow, Glasgow G12 8QQ, United Kingdom

Edited by Hiroshi Nikaido, University of California, Berkeley, CA, and approved September 28, 2017 (received for review August 3, 2017)

Unlike their descendants, mitochondria and plastids, bacteria do not have dedicated protein import systems. However, paradoxically, import of protein bacteriocins, the mechanisms of which are poorly understood, underpins competition among pathogenic and commensal bacteria alike. Here, using X-ray crystallography, isothermal titration calorimetry, confocal fluorescence microscopy, and in vivo photoactivatable cross-linking of stalled translocation intermediates, we demonstrate how the iron transporter FpvAI in the opportunistic pathogen *Pseudomonas aeruginosa* is hijacked to translocate the bacteriocin pyocin S2 (pyoS2) across the outer membrane (OM). FpvAI is a TonB-dependent transporter (TBDT) that actively imports the small siderophore ferripyoverdine (Fe-Pvd) by coupling to the proton motive force (PMF) via the inner membrane (IM) protein TonB1. The crystal structure of the N-terminal domain of pyoS2 ($pyoS2^{NTD}$) bound to FpvAI (K_d = 240 pM) reveals that the pyocin mimics Fe-Pvd, inducing the same conformational changes in the receptor. Mimicry leads to fluorescently labeled $pyoS2^{NTD}$ being imported into FpvAI-expressing *P. aeruginosa* cells by a process analogous to that used by bona fide TBDT ligands. $PyoS2^{NTD}$ induces unfolding by TonB1 of a force-labile portion of the plug domain that normally occludes the central channel of FpvAI. The pyocin is then dragged through this narrow channel following delivery of its own TonB1-binding epitope to the periplasm. Hence, energized nutrient transporters in bacteria also serve as rudimentary protein import systems, which, in the case of FpvAI, results in a protein antibiotic 60-fold bigger than the transporter's natural substrate being translocated across the OM.

Pseudomonas aeruginosa | pyocin | outer membrane receptor | transporter

Bacteriocins are peptide or protein antibiotics produced by bacteria to kill their neighbors, usually in response to environmental stress, that play a fundamental role in shaping bacterial communities (1–3) and are implicated in the invasion mechanisms of pathogens (4, 5). Bacteriocins are currently the focus of intense efforts to develop them as much needed antibiotics against multidrug-resistant bacteria (6, 7) and as antiinfectives for use in agriculture (8). The present work centers on the mode of action of protein bacteriocins, which are species-specific protein antibiotics that are widespread agents of competition in gram-negative bacteria (9). Protein bacteriocins are known to parasitize a variety of cell envelope proteins (10), but how they exploit these systems to promote their import has remained unresolved since their discovery (11). We reveal the mechanism by which the nuclease bacteriocin pyocin S2 (pyoS2) crosses the outer membrane (OM) of *Pseudomonas aeruginosa*, a path that is likely to be used by other TonB-dependent protein bacteriocins.

Protein bacteriocins are 40- to 80-kDa toxins that carry a single cytotoxic domain at their C terminus into the cell. Cell death ensues through depolarization of the cell by an ionophore or enzymatic cleavage of peptidoglycan precursors in the periplasm or nucleic acids (DNA, tRNA, or rRNA) in the cytoplasm (12). The best studied of the protein bacteriocins are the colicins that target and kill *Escherichia coli*. Colicins exploit a variety of OM proteins as their primary receptor, including the vitamin B_{12} transporter BtuB and the siderophore transporter FepA (13, 14). Colicin entry into cells requires contact with proton motive force (PMF)-linked systems in the inner membrane (IM) that span the periplasm: Tol-Pal for group A colicins and Ton for group B colicins (15). Tol-Pal is a multiprotein complex involving three IM proteins (TolA, TolQ, and TolR), a periplasmic protein (TolB), and an OM lipoprotein (Pal). The Ton system comprises three IM proteins (TonB, ExbB, and ExbD). Both systems, which are virulence factors in pathogenic bacteria, energize processes at the OM: Tol-Pal stabilizes the membrane, while Ton catalyzes import of scarce nutrients such as iron and vitamins across the membrane. Group A colicins generally require additional OM proteins, usually porins, to contact the Tol-Pal system (16). Few translocator proteins have been identified for group B colicins (10). How the Ton or Tol-Pal system catalyzes import of a protein bacteriocin across the OM is unknown. Once in the periplasm, nuclease colicins are translocated across the IM by the AAA^+ ATPase FtsH, which also proteolytically releases the nuclease domain to the cytoplasm (17, 18). In the present work, we reveal how pyoS2, a Ton-dependent protein bacteriocin, translocates across the OM through its receptor and show that this mechanism has strong parallels with that used by the endogenous ligand for the receptor.

Significance

The outer membrane (OM) excludes antibiotics such as vancomycin that kill gram-positive bacteria, and so is a major contributor to multidrug resistance in gram-negative bacteria. Yet, the OM is readily bypassed by protein bacteriocins, which are toxins released by bacteria to kill their neighbors during competition for resources. Discovered over 60 y ago, it has been a mystery how these proteins cross the OM to deliver their toxic payload. We have discovered how the bacteriocin pyocin S2 (pyoS2), which degrades DNA, enters *Pseudomonas aeruginosa* cells. PyoS2 tricks the iron transporter FpvAI into transporting it across the OM by a process that is remarkably similar to that used by its endogenous ligand, the siderophore ferripyoverdine.

Author contributions: P.W., A.J., N.G.H., and C.K. designed research; P.W., P.R., N.G.H., J.D.G., C.R., and S.M. performed research; P.W., N.G.H., R.K., L.C.M., and D.W. contributed new reagents/analytic tools; P.W., A.J., P.R., N.G.H., J.D.G., C.R., and S.M. analyzed data; and P.W., C.R., and C.K. wrote the paper.

The authors declare no conflict of interest.

This article is a PNAS Direct Submission.

Data deposition: The atomic coordinates and structure factors have been deposited in the Protein Data Bank, www.wwpdb.org (PDB ID code 5ODW).

[1]Present address: Lonza Biologics Plc, Slough SL1 4DX, United Kingdom.

[2]To whom correspondence should be addressed. Email: colin.kleanthous@bioch.ox.ac.uk.

This article contains supporting information online at www.pnas.org/lookup/suppl/doi:10.1073/pnas.1713741114/-/DCSupplemental.

Results

The N-Terminal Domain of PyoS2 Mimics Ferripyoverdine Binding to FpvAI. PyoS2 is a 74-kDa endonuclease bacteriocin that is effective in the treatment of *P. aeruginosa*-induced pneumonia in mice and in eradicating *P. aeruginosa* biofilms (6, 19). The primary receptor for pyoS2 is FpvAI (20–22), a TonB-dependent transporter (TBDT) (23) that actively imports ferripyoverdine (Fe-Pvd) (24). FpvAI is a classical 22-stranded β-barrel with a central channel that is completely occluded by a globular "plug" domain, which must be reconfigured for substrate transport by coupling to the PMF via TonB1 (25).

Our starting point for elucidating the pyoS2 mechanism of entry was to delineate the FpvAI-binding domain by limited trypsin digestion (residues 1–209; *Materials and Methods*). The isolated 23-kDa N-terminal domain of pyoS2 (pyoS2^{NTD}) was folded (Fig. S1*A*) and outcompeted Fe-Pvd for FpvAI (Fig. 1*A*), which it bound with high affinity in competition isothermal titration calorimetry (ITC) experiments (K_d = 240 pM) (Fig. 1*B*). We solved the crystal structure of the FpvAI–pyoS2^{NTD} complex by molecular replacement to a resolution of 2.8 Å (details are provided in *Materials and Methods*). Continuous electron density was observed for residues 11–208 of the pyoS2^{NTD}, and near-complete density was observed for FpvAI (Fig. 1*C* and Table S1). PyoS2^{NTD} is composed of five α-helices, including a C-terminal helix extending ∼80 Å from the interface and a short antiparallel β-hairpin at the N terminus (residues 11–26) that docks onto the helical bundle. Spectroscopic measurements indicated that this N-terminal region is folded in solution and contributes to the stability of the domain, but high B-factors in the crystal structure suggest this region is likely to be dynamic (Fig. S1). An 11-amino acid proline-rich region (PRR; residues 35–45) contacts primarily the FpvAI plug domain. Deletion of the first 45 residues, including the PRR (Δ1–45 pyoS2^{NTD}), decreased pyoS2^{NTD} binding ∼1,000-fold (Fig. S2). Importantly, the PRR not only occupies the same binding site as Fe-Pvd but also resembles its shape (Fig. 1 *D* and *E* and Fig. S3*A*). Consequently, pyoS2^{NTD} induces conformational changes within the plug that are very similar to those triggered by Fe-Pvd, as evidenced by comparable backbone rmsds for the two complexes relative to unliganded receptor and by the equivalent reconfiguring of the same secondary structure elements (Fig. S3 *B–E*). In summary, the structure of the complex points to pyoS2 exploiting FpvAI both as a receptor and translocator, in contrast to bacteriocins that recruit additional OM proteins for import (3).

PyoS2^{NTD} Translocates into *P. aeruginosa* Cells. We developed a fluorescence-based assay using Alexa Fluor 488-conjugated pyoS2^{NTD} (pyoS2^{NTD}-AF488) to probe pyoS2^{NTD} import in vivo. Addition of pyoS2^{NTD}-AF488 to live *P. aeruginosa* PAO1 cells yielded fluorescent bacteria, whereas those lacking FpvAI were not labeled (Fig. 2*A*). Fluorescence recovery after photobleaching (FRAP) was used to monitor pyoS2^{NTD}-AF488 translocation. Since OM proteins have restricted lateral diffusion (26), the expectation was that pyoS2^{NTD}-AF488 bound to FpvAI would not show fluorescence recovery in FRAP experiments. Instead, we observed rapid fluorescence recovery (Fig. 2*B*), suggesting pyoS2^{NTD}-AF488 was translocating to the periplasm, where it could diffuse freely. We investigated the energetics of import as a test of this hypothesis. Dissipation of the PMF by the addition of the protonophore carbonyl cyanide *m*-chlorophenyl hydrazone (CCCP) to *P. aeruginosa* before labeling with pyoS2^{NTD}-AF488 resulted in no recovery of fluorescence in FRAP experiments (Fig. 2*C*), consistent with pyoS2^{NTD}-AF488 remaining bound to FpvAI in the OM of a deenergized cell. TBDT ligands are transported through their receptors in conjunction with the PMF, which is transduced into mechanical force by engagement of the IM protein TonB with a TonB box motif of the transporter (23) (Fig. 1*C*). The TonB box of

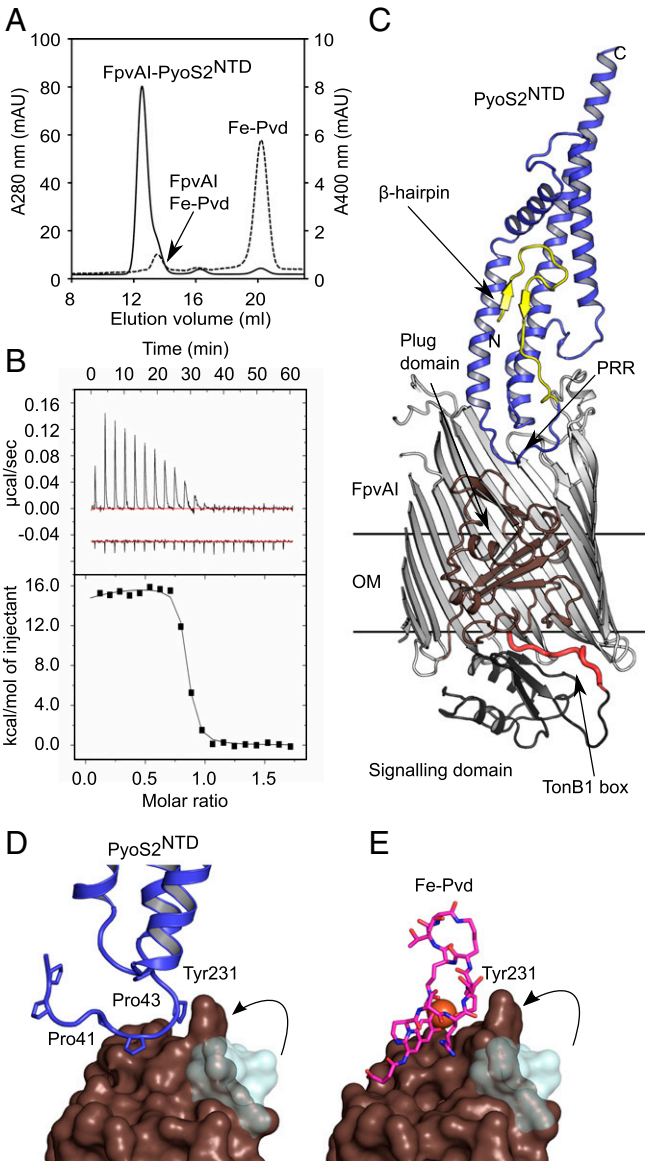

Fig. 1. High-affinity binding of pyoS2^{NTD} to FpvAI mimics that of Fe-Pvd. (*A*) PyoS2^{NTD} outcompetes Fe-Pvd for FpvAI binding in analytical gel-filtration chromatography. Protein elution was monitored at A_{280} (solid line), and Fe-Pvd elution was monitored at A_{400} (dashed line). mAu, milliabsorbance units. (*B*) ITC data for pyoS2^{NTD} binding FpvAI in the presence of a lower affinity competitor, Δ1–45 pyoS2^{NTD} (details are provided in *Materials and Methods*). Data from two independent experiments were fitted to a competitive binding model from which the following thermodynamic parameters were extracted: $\Delta H = -15.8 \pm 1.4$ kcal/mol, $\Delta S = -9.1 \pm 4.6$ cal·mol^{-1}·K^{-1}, n = 0.78 ± 0.02 sites, $K_d = 0.24 \pm 0.004 \times 10^{-9}$ M. (*C*) The 2.8-Å crystal structure of pyoS2^{NTD} (blue) in complex with FpvAI (gray) highlighting the pyoS2^{NTD} β-hairpin (yellow), the FpvAI plug (brown) and signaling domains (black), and the TonB1 box (red). Several of the β-strands that make up the β-barrel of FpvAI have been removed to highlight the plug domain. The signaling domain of FpvAI is involved in activating its own expression and that of Pvd (41). (*D* and *E*) Comparison of FpvAI plug domain surface when bound by the PRR of pyoS2^{NTD} and Fe-Pvd, respectively, highlighting the movement of FpvAI Tyr231 from its position in the unliganded state (light blue).

FpvAI is known to be required for both Fe-Pvd import and pyoS2 toxicity (27). Of the three *tonB* genes in *P. aeruginosa*, only *tonB1* was required for pyoS2 toxicity (Fig. S4*A*), as has been reported for Fe-Pvd import (28). We also identified a putative TonB box at the N terminus of pyoS2^{NTD} (M^{11}VITH^{15}) that comprises the

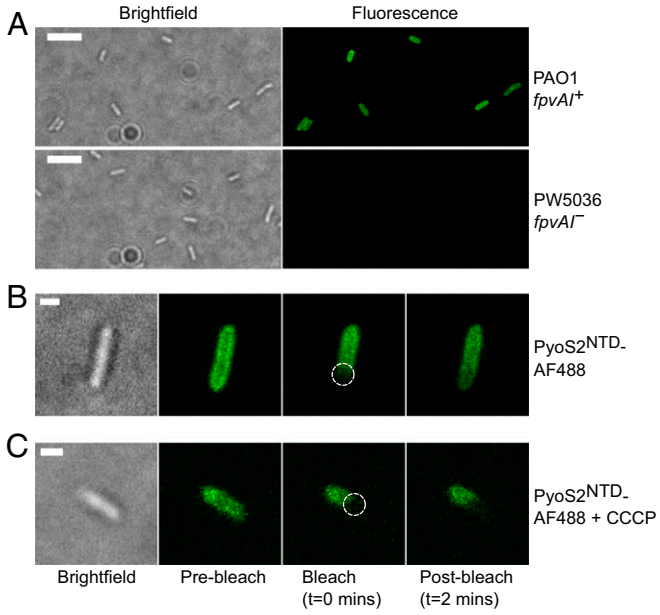

Fig. 2. PyoS2^{NTD} translocates across the *P. aeruginosa* OM. (*A*) Fluorescence labeling of live FpvAI-expressing *P. aeruginosa* PAO1 with pyoS2^{NTD}-AF488. The PAO1 *fpvA*$^{-}$ transposon mutant PW5036 (*fpvA*-H02::ISlacZ/hah) exhibits no labeling. (Scale bars, 5 μm.) FRAP experiments on *P. aeruginosa* PAO1 labeled with pyoS2^{NTD}-AF488 (*B*) and pyoS2^{NTD}-AF488 (*C*) are shown, where cells were first treated with 100 μM CCCP. The bleached region is highlighted (dashed circle). The absence of FRAP in these experiments suggests pyoS2^{NTD} remains bound to FpvAI in the OM, whereas FRAP suggests pyoS2^{NTD}-AF488 has translocated to the periplasm, where it can diffuse laterally. (Scale bars, 1 μm.)

first β-strand of the β-hairpin. TonB-dependent bacteriocins such as colicin B, which targets *E. coli*, generally have their own TonB box (29). Direct binding of pyoS2^{NTD} to TonB1 was shown by ITC ($K_d \sim 1$ μM), as well as by cross-linking, and was abolished when the β-hairpin was deleted (Δ1–30 pyoS2^{NTD}) (Fig. S4 *B–D*). Deletion of the TonB1 box (Δ1–21 pyoS2^{NTD}-AF488) also abolished fluorescence recovery in FRAP experiments, as well as pyoS2 cytotoxicity (Fig. S5 *A* and *B*). Finally, Δ1–21 pyoS2^{NTD}-AF488 fluorescence, when bound to cells, was completely removed by trypsin treatment, in contrast to pyoS2^{NTD}-AF488 (Fig. S5 *C–E*). We conclude that as well as being the receptor-binding domain for the bacteriocin, pyoS2^{NTD} carries all of the information necessary for translocation across the OM and that the process requires at least FpvAI, the PMF, and TonB1 in the IM. Thereafter, import to the cytoplasm is mediated by the bacteriocin nuclease domain FtsH and a conserved DPY motif present in all nuclease bacteriocins (9, 17, 30).

PyoS2^{NTD} Translocation Through FpvAI Mirrors That of a TBDT Ligand. We developed a cross-linking strategy to map the pyoS2 import route that capitalized on its PMF dependence and involved trapping pyoS2^{NTD} during translocation. The PMF delivers ∼20 pN mechanical force (31), and so we fused pyoS2^{NTD} to GFP (pyoS2^{NTD}-GFP), which can resist up to 100 pN (32). In contrast to pyoS2^{NTD}-AF488, FRAP experiments with pyoS2^{NTD}-GFP bound to *P. aeruginosa* cells did not show fluorescence recovery, consistent with a block in translocation (Fig. 3*A*). We substituted 13 pyoS2^{NTD} residues, distributed throughout the pyoS2^{NTD}-GFP construct, for the UV-inducible cross-linker *para*-Benzoylphenylalanine (*p*Bpa) (*Materials and Methods* and Fig. 3*B*). The interfacial site Tyr46*p*Bpa was included as a positive control. All *p*Bpa variants were purified and first complexed with FpvAI in vitro. Of the 13 variants, cross-linking was only observed for Tyr46*p*Bpa, its cross-link to FpvAI Met431 at the protein–protein interface confirmed by liquid chromatography-tandem mass spectrometry (LC-MS/MS) (Fig. S6). After ensuring *p*Bpa labeling did not interfere with pyoS2 cytotoxicity (Fig. S4*E*), we developed a method for cross-linking and purifying pyoS2^{NTD}-GFP translocation intermediates from live *P. aeruginosa* cells and identified cross-linking sites by LC-MS/MS (*Materials and Methods*). In vivo cross-links were observed for all 13 *p*Bpa variants, suggesting that translocation intermediates were indeed trapped by this strategy (Fig. 3*C*). We were able to map cross-links for seven *p*Bpa sites (Gln17, Ile23, Ala29, Lys70, Ala87, Gln135, and Gln184), all of which were to transmembrane regions of FpvAI that are inaccessible to pyoS2^{NTD} in its ground state complex with FpvAI (Fig. 1*C*). PyoS2^{NTD} must translocate significant distances to satisfy the cross-linking data, as in the case of pyoS2^{NTD} Gln184, which moves 76 Å to meet FpvAI Val197 (Fig. 3 *B–D*). We identified six principal cross-link sites in FpvAI, although LC-MS/MS data suggested residues to either side of these sites are also hit, but at lower frequency (Figs. S7 and S8). Five of six residues are within the plug domain that occludes the channel, and one was to the barrel wall (Met766) (Fig. 3*B*). Four *p*Bpa sites (Gln17, Ile23, Ala87, and Gln135) cross-link to the same FpvAI plug domain residue, Met177, suggesting much of the pyoS2^{NTD} polypeptide chain translocates past this residue.

We have interpreted our cross-linking data in the context of recent atomic force microscopy (AFM) studies on other TBDTs, the vitamin B_{12} transporter BtuB, and the ferric hydroxamate receptor FhuA from *E. coli* (Fig. 4). Hickman et al. (33) have shown that the plug domains of BtuB and FhuA are composed of force-resistant and force-labile subdomains. Displacement of the force-labile subdomain by engagement of TonB with the ligand-bound transporter opens an ∼13-Å-wide channel. Structural alignment of the plug domains of BtuB (34) and FpvAI identifies an equivalent force-labile subdomain (Fig. S9). PyoS2^{NTD} translocation therefore involves at least three steps (Fig. 4). Step 1 is binding of pyoS2^{NTD} to FpvAI, where Fe-Pvd mimicry induces recruitment of TonB1 in the periplasm. Step 2 is PMF-driven unfolding of the FpvAI force-labile subdomain, release of the N-terminal β-hairpin, and delivery of the pyocin's TonB1 box through the channel, where it engages either the same or another copy of TonB1. The *p*Bpa substitutions at pyoS2^{NTD} residues Gln17, Ile23, and Ala29 all cross-link to sites within the channel, either to the nonlabile subdomain (Asp239) or to the barrel wall (Met766). Displacement of the β-hairpin from the helical bundle of pyoS2^{NTD} destabilizes the domain (Fig. S1*C*), expediting import. Step 3 is TonB1-dependent unfolding of pyoS2^{NTD}. The majority of observed cross-links are for this final state in which five pyoS2^{NTD} residues spanning >100 amino acids become cross-linked to three hyperreactive FpvAI labile subdomain residues (Pro166, Met177, and Leu182). PyoS2^{NTD} residues Gln17 and Ile23 are among the sites that cross-link to FpvAI Met177, which, along with their cross-links to Met776, explains why these residues give two cross-linked adducts on SDS/PAGE (Fig. 3*C*). Finally, a single cross-link was observed between pyoS2^{NTD} Gln184*p*Bpa and FpvAI Val197, likely denoting the entrapment by GFP of the translocating pyocin within the FpvAI channel.

Discussion

Our data show that PMF-coupled TonB1 imports pyoS2^{NTD} by dragging it through a narrow channel in FpvAI created by TonB1-induced displacement of the labile plug subdomain, a pathway ordinarily used by its ligand Fe-Pvd. TBDT plug displacement is thought to be facilitated by waters at the plug–barrel interface, which could lubricate pyoS2 translocation (35). Two mechanisms seem reasonable as to how the remaining ∼500 amino acids of pyoS2 translocate through FpvAI; either the PMF continues to be involved or refolding of pyoS2^{NTD} in the periplasm provides the driving force. Force-dependent unfolding of

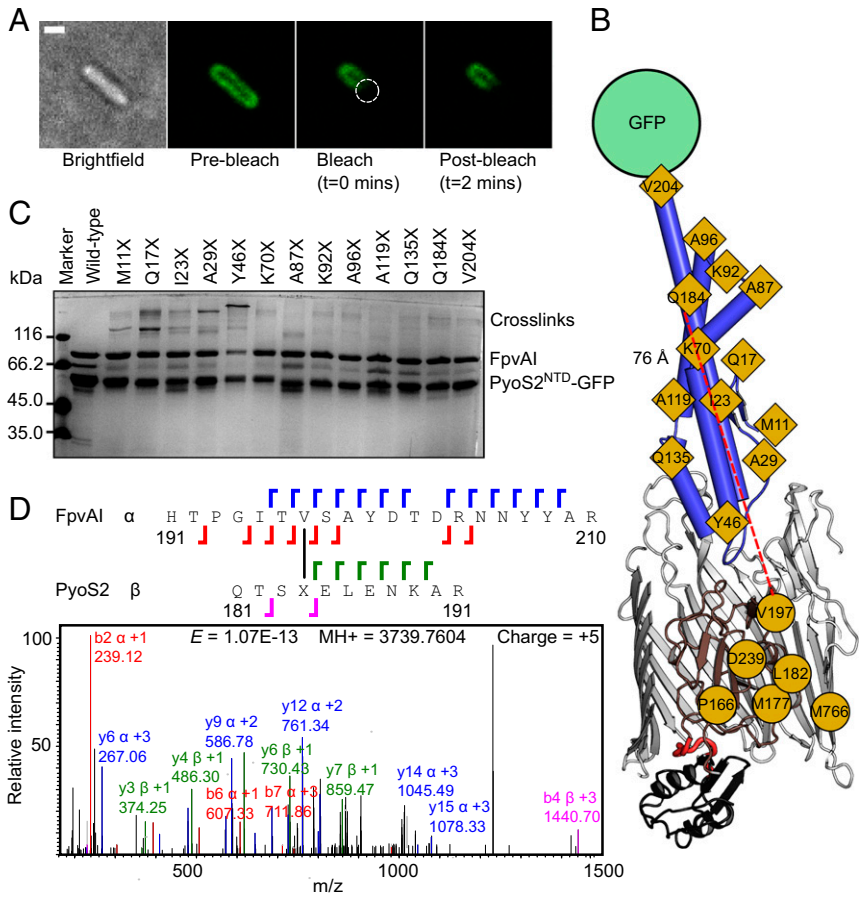

Fig. 3. Mapping the pyoS2^{NTD} translocation pathway by photo cross-linking. (*A*) FRAP experiment on a *P. aeruginosa* PAO1 cell labeled with pyoS2^{NTD}-GFP demonstrates stalled import. The bleached region is highlighted (dashed circle). (Scale bar, 1 μm.) (*B*) Structure of the pyoS2^{NTD}–FpvAI complex showing the sites of *p*Bpa incorporation in pyoS2^{NTD}-GFP (yellow diamonds) and the major cross-link sites in FpvAI (yellow circles), most of which are located in the plug domain of the TBDT. The red dotted line indicates the cross-link detected between *p*Bpa184 in pyoS2^{NTD} and Val197 in FpvAI, which requires this region of the pyocin to translocate at least 76 Å. (*C*) Ten percent SDS/PAGE gel showing Coomassie-stained, in vivo cross-linked adducts of translocated pyoS2^{NTD}-GFP*p*Bpa variants following purification by nickel affinity chromatography from OM extracts of *P. aeruginosa* PAO1 cells. Only cross-links to FpvAI were observed by LC-MS/MS, confirming that GFP traps the translocating pyoS2^{NTD} within FpvAI (details are provided in *Materials and Methods*). (*D*) Fragmentation spectrum of *p*Bpa184-Val197 cross-linked peptides (X = *p*Bpa) with *b*- and *y*-ions indicated, along with the *E*-value, precursor ion mass (MH+), and precursor ion charge.

the bacteriocin during import disrupts the high-affinity complexes of the pyocin with FpvAI ($K_d \simeq$ pM) and the C-terminal nuclease with its immunity protein ($K_d \simeq$ fM) (36). Immunity proteins protect nuclease bacteriocin-producing cells but are displaced at the cell surface during import (37). AFM studies have shown that force-dependent remodeling of a colicin nuclease accelerates the immunity protein dissociation rate (31). PyoS2 unfolding during import could provide this remodeling force. Ton-dependent bacteriocins are widely distributed in bacteria, delivering different cytotoxic activities (nucleases, peptidoglycan hydrolases, and ionophores) (12). The subversion of FpvAI by pyoS2 demonstrates a mechanism that is likely to be the basis of import for many Ton-dependent bacteriocins and reveals how TBDTs moonlight as protein transporters.

The protein import mechanism we have uncovered in bacteria has similarities to the classical protein import pathway of mitochondria catalyzed by the translocase at outer membrane complex (38). Both systems rely on an N-terminal sequence motif, the presequence in mitochondria and the TonB box in bacteria, for translocation across the OM. These sequences direct protein import through β-barrel transporters, driven by protein complexes in the IM coupled to the PMF. Unlike mitochondria, however, where the presequence is recognized by a receptor within the translocase, in bacteria, the imported proteins themselves are recognized by specific receptors that also act as translocases.

Materials and Methods

Protein Expression and Purification. His-tagged pyoS2^{NTD} and derivatives were expressed in BL21 (DE3) cells and were purified by nickel-affinity chromatography and size-exclusion chromatography (SEC). The TonB1 periplasmic domain (residues 109–342) was purified using the same method with the addition of tobacco etch virus-protease removal of the His-tag. FpvAI was expressed in *E. coli* TNE012 cells (*ompA*$^-$, *ompB*$^-$, and *tsx*$^-$) (39) transformed with pNGH183 carrying the *fpvAI* gene from *P. aeruginosa* PAO1 with an *E. coli ompF* signal sequence. After isolation of the OM fraction, FpvAI was purified by anion exchange chromatography and SEC. Details are described in *Supporting Information*.

Limited Trypsin Proteolysis and Peptide Mass Fingerprinting. A total of 2 mg of full-length pyoS2 (purified using the same method as described for the pyoS2^{NTD}) in a 1:1 molar complex with FpvAI was digested with 2 μg of Sequencing Grade Modified Trypsin (Promega) at room temperature overnight in 25 mM Tris·HCl (pH 8.0), 150 mM NaCl, and 1% (wt/vol) *n*-octyl-β-D-glucopyranoside (β-OG). Digestion was stopped with 1 mM PMSF, and fragments were copurified with FpvAI on a Superdex 200 10/300 GL column (GE Healthcare). Fragments were resolved by SDS/PAGE, and bands were excised for in-gel trypsin digestion and peptide mass fingerprinting as described in *Supporting Information*.

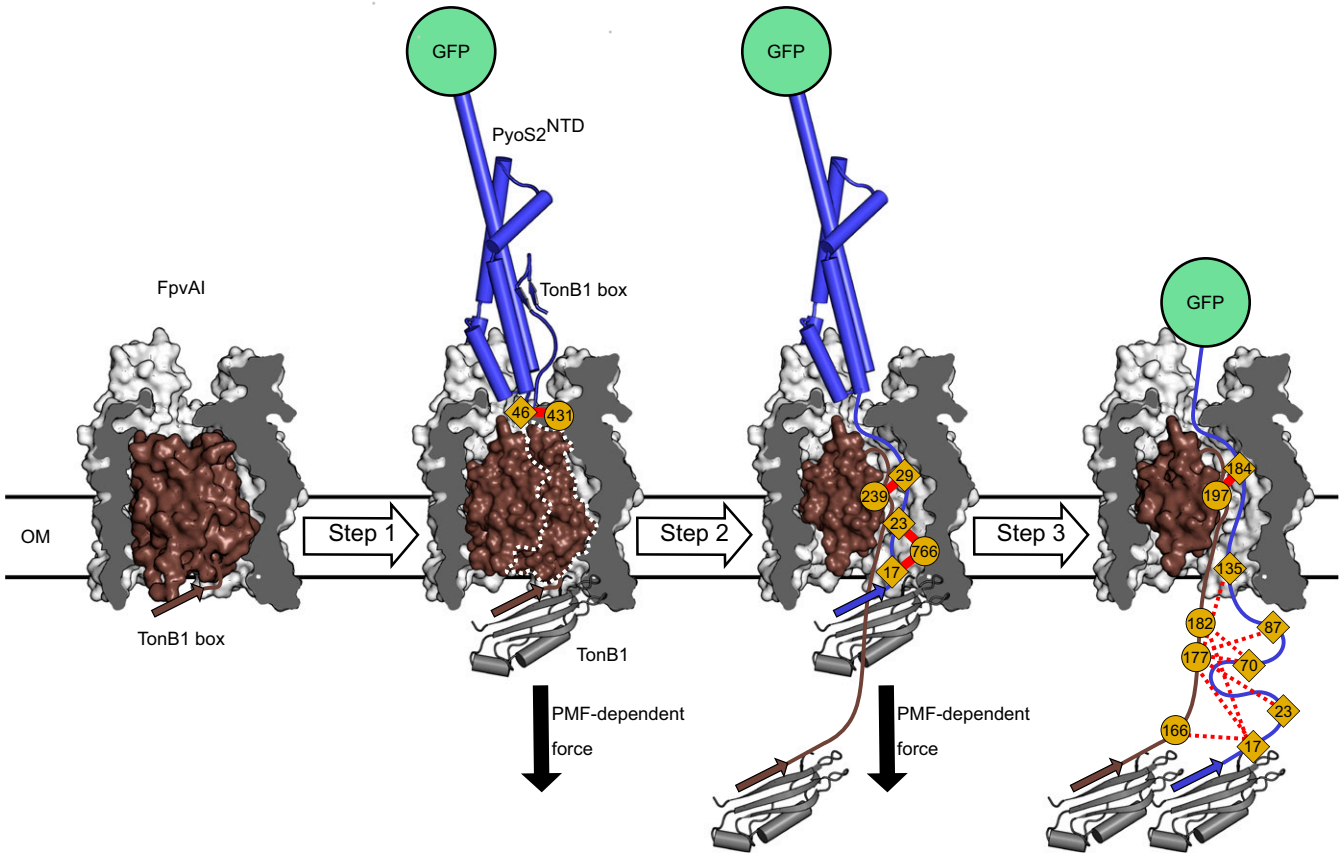

Fig. 4. Model for pyoS2^{NTD} translocation through FpvAI. The three-step model of pyoS2^{NTD} translocation through FpvAI supported by *p*Bpa cross-linking data (Fig. 3 and Figs. S6–S9) is shown. In step 1, binding of pyoS2^{NTD} to FpvAI mimics Fe-Pvd, activating the receptor for substrate transport and recruiting the C-terminal domain of TonB1 in the periplasm. In step 2, a PMF-dependent mechanical force, applied via the ExbB–ExbD–TonB1 complex in the IM (not shown), drives unfolding of the labile half of the plug domain. The N terminus of pyoS2^{NTD} enters the ∼13-Å-wide cavity that is created, allowing it to present its own TonB1 box in the periplasm. In step 3, the pyoS2^{NTD} TonB1 box is bound by another copy of TonB1; at this time, the mechanical force is used to drive translocation of pyoS2^{NTD} through the FpvAI lumen. Further translocation is blocked by the force-resistant GFP. The multiple cross-links observed between the labile portion of the FpvAI plug domain and translocated pyoS2^{NTD} residues are presumed to involve unfolded polypeptide chains in the periplasm.

Analytical SEC. PyoS2^{NTD} at 5 μM was added to a 5 μM stoichiometric complex of FpvAI and Fe-Pvd (Sigma) in 25 mM Tris·HCl (pH 8.0), 150 mM NaCl, and 1% (wt/vol) β-OG, and was incubated at room temperature for 6 h. The mixture was separated on a Superdex 200 10/300 GL column equilibrated in the same reaction buffer monitoring for protein elution at A_{280} and for Fe-Pvd elution at A_{400}.

Crystallization and Structure Determination. The FpvAI–pyoS2^{NTD} complex at 8 mg/mL, purified as described in *Supporting Information*, was crystallized by the sitting-drop vapor diffusion method in 96-well MRC two-drop plates (SWISSCI) at 18 °C. Drops consisted of 100 nL of protein and 100 nL of crystallization solution dispensed using a Mosquito robot (TTP Labtech). Crystals of the complex were grown in 0.35 M ammonium sulfate, 13.5% (wt/vol) PEG3350, and 0.05 M sodium acetate (pH 4.0), and were harvested after 30 d. Crystals were cryoprotected in the crystallization solution supplemented with 1% (vol/vol) *n*-octyl-polyoxyethylene and 25% (vol/vol) ethylene glycol before flash-cooling into liquid nitrogen. X-ray data were collected at the European Synchrotron Radiation Facility on beamline ID23-2 from a single cryocooled crystal (100 K) using a 225-mm MarMOSAIC CCD detector. Data collection, processing, refinement, and model building are described in *Supporting Information*. The atomic coordinates and structure factors for the pyoS2^{NTD}–FpvAI complex [Protein Data Bank (PDB) ID code 5ODW] have been deposited in the PDB.

Fluorescence Microscopy. Alexa Fluor 488 was conjugated onto the C terminus of pyoS2^{NTD} as described in *Supporting Information*. *P. aeruginosa* PAO1 cells were grown in M9-glucose media (6.78 g/L Na_2HPO_4, 3 g/L KH_2PO_4, 0.5 g/L NaCl, 10 mM D-glucose, 1 mg/mL NH_4Cl, 2 mM $MgSO_4$) at 37 °C, and were labeled with 1 μM fluorophore-conjugated pyoS2 construct for 15 min (details are provided in *Supporting Information*). FRAP experiments were performed using a PerkinElmer spinning disk confocal microscope with a 100× oil-immersion objective (1.4 N.A.). Images were acquired using the 488-nm laser at 10% power, and bleaching was performed at 50% laser power at maximum speed. Recovery images were acquired over a time course up to 2 min. Bright-field images were recorded for each FRAP experiment.

ITC. For FpvAI-pyoS2^{NTD}–binding experiments, proteins were prepared in 50 mM potassium phosphate (pH 7.0) and 1% (wt/vol) β-OG. Experiments were performed using a MicroCal iTC$_{200}$ thermostat at 25 °C. The cell contained FpvAI at 3.5 μM, and the syringe contained pyoS2^{NTD} at 70 μM. Competition ITC experiments were performed with 10 μM FpvAI and 15 μM Δ1–45 pyoS2^{NTD} in the cell and with 70 μM pyoS2^{NTD} in the syringe. Because of the small ΔH, TonB1-pyoS2^{NTD}–binding experiments were performed using a MicroCal PEAQ-ITC isothermal titration calorimeter. Proteins were prepared in 50 mM potassium phosphate (pH 7.0) and 150 mM NaCl. The cell contained TonB1 at 15 μM, and the syringe contained either pyoS2^{NTD} or Δ1–30 pyoS2^{NTD} at 150 μM. The first injection of 0.5 μL was followed by 19 injections of 2 μL, with each injection spaced by 180 s. Binding isotherms were fitted using the manufacturer's software.

Growth Inhibition Assays. PyoS2 cytotoxic activity was assayed by plate-based growth inhibition assays. Typically, a 10-mL culture of *P. aeruginosa* was grown at 37 °C to an OD_{600} of 0.6. Lawns were prepared by addition of 200 μL of culture to 5 mL of molten soft LB-agar [0.75% (wt/vol) agar in LB] at 42 °C and were poured over LB-agar plates. Once set and dry, 2 μL of serially diluted wild-type or variant pyoS2 was applied to the lawn. Lawns were allowed to grow overnight at 37 °C, and cytotoxicity was determined by observation of clearance zones.

LC-MS/MS Identification of in Vivo Photoactivated Cross-Links. A 500-mL culture of *P. aeruginosa* PAO1 was grown for 24 h at 30 °C in iron-free succinate medium (6.1 g/L K_2HPO_4, 3 g/L KH_2PO_4, 4.1 g/L succinic acid) supplemented with 7.5 mM $(NH_4)_2SO_4$, 1 mM $MgSO_4$, and 1× trace metal solution [prepared as PTM4(Fe^-) as described elsewhere (40)]. Cells were washed and resuspended in 35 mL of fresh medium, incubated for 60 min in the presence of 100 nM pyoS2^{NTD}-GFP*p*Bpa variants, and UV-irradiated at 365 nm for 30 min in a CL-1000 UV cross-linker. Cells were then resuspended in 10 mM Tris·HCl (pH 8.0), 0.25% (wt/vol) lithium diiodosalicyclic acid, and 2% (vol/vol) Triton X-100, and were lysed through sonication. The cleared lysate was ultracentrifuged at 200,000 × *g* for 45 min to isolate the OM fraction, which was solubilized in 10 mM Tris·HCl (pH 8.0), 5 mM EDTA, and 2% (wt/vol) β-OG. Cross-linked complexes were purified using EDTA-resistant cOmplete His-Tag Purification Resin (Roche) and were resolved by SDS/PAGE. Cross-linking sites were mapped by LC-MS/MS and pLink software as described in *Supporting Information*.

ACKNOWLEDGMENTS. We thank Iain Lamont for kindly providing the *tonB* mutant and parent strains PAO6609, K1040, K1407, and MS231. We thank Svenja Hester for preparing cross-linking gel slices for LC-MS/MS. We thank Ed Lowe and European Synchrotron Radiation Facility ID23-2 beamline staff for assistance with X-ray data collection, and we thank David Staunton for assistance with molecular biophysics measurements. This work was funded by the Wellcome Trust (Grant 201505/Z/16/Z) and Biotechnology and Biological Sciences Research Council (Grant BB/G020671/2). P.W. was funded by the Wellcome Trust Doctoral Training Centre for Cellular and Structural Biology. We acknowledge Grant NIH P30 DK089507 for use of the two-allele library strain PW5036.

1. Kirkup BC, Riley MA (2004) Antibiotic-mediated antagonism leads to a bacterial game of rock-paper-scissors in vivo. *Nature* 428:412–414.
2. Wiener M, Freymann D, Ghosh P, Stroud RM (1997) Crystal structure of colicin Ia. *Nature* 385:461–464.
3. Housden NG, et al. (2013) Intrinsically disordered protein threads through the bacterial outer-membrane porin OmpF. *Science* 340:1570–1574.
4. Nedialkova LP, et al. (2014) Inflammation fuels colicin Ib-dependent competition of *Salmonella* serovar *Typhimurium* and *E. coli* in enterobacterial blooms. *PLoS Pathog* 10:e1003844.
5. Holt KE, et al. (2013) Tracking the establishment of local endemic populations of an emergent enteric pathogen. *Proc Natl Acad Sci USA* 110:17522–17527.
6. McCaughey LC, Ritchie ND, Douce GR, Evans TJ, Walker D (2016) Efficacy of species-specific protein antibiotics in a murine model of acute *Pseudomonas aeruginosa* lung infection. *Sci Rep* 6:30201.
7. Cotter PD, Ross RP, Hill C (2013) Bacteriocins - A viable alternative to antibiotics? *Nat Rev Microbiol* 11:95–105.
8. Schulz S, et al. (2015) Broad and efficient control of major foodborne pathogenic strains of Escherichia coli by mixtures of plant-produced colicins. *Proc Natl Acad Sci USA* 112:E5454–E5460.
9. Sharp C, Bray J, Housden NG, Maiden MCJ, Kleanthous C (2017) Diversity and distribution of nuclease bacteriocins in bacterial genomes revealed using Hidden Markov Models. *PLOS Comput Biol* 13:e1005652.
10. Kleanthous C (2010) Swimming against the tide: Progress and challenges in our understanding of colicin translocation. *Nat Rev Microbiol* 8:843–848.
11. Fredericq P (1957) Colicins. *Annu Rev Microbiol* 11:7–22.
12. Braun V, Patzer SI, Hantke K (2002) Ton-dependent colicins and microcins: Modular design and evolution. *Biochimie* 84:365–380.
13. Kurisu G, et al. (2003) The structure of BtuB with bound colicin E3 R-domain implies a translocon. *Nat Struct Biol* 10:948–954.
14. Devanathan S, Postle K (2007) Studies on colicin B translocation: FepA is gated by TonB. *Mol Microbiol* 65:441–453.
15. Cascales E, et al. (2007) Colicin biology. *Microbiol Mol Biol Rev* 71:158–229.
16. Housden NG, et al. (2010) Directed epitope delivery across the Escherichia coli outer membrane through the porin OmpF. *Proc Natl Acad Sci USA* 107:21412–21417.
17. Walker D, Mosbahi K, Vankemmelbeke M, James R, Kleanthous C (2007) The role of electrostatics in colicin nuclease domain translocation into bacterial cells. *J Biol Chem* 282:31389–31397.
18. Chauleau M, Mora L, Serba J, de Zamaroczy M (2011) FtsH-dependent processing of RNase colicins D and E3 means that only the cytotoxic domains are imported into the cytoplasm. *J Biol Chem* 286:29397–29407.
19. Smith K, et al. (2012) Activity of pyocin S2 against *Pseudomonas aeruginosa* biofilms. *Antimicrob Agents Chemother* 56:1599–1601.
20. Ohkawa I, Shiga S, Kageyama M (1980) Effect of iron concentration in the growth medium on the sensitivity of *Pseudomonas aeruginosa* to pyocin S2. *J Biochem* 87: 323–331.
21. Denayer S, Matthijs S, Cornelis P (2007) Pyocin S2 (Sa) kills *Pseudomonas aeruginosa* strains via the FpvA type I ferripyoverdine receptor. *J Bacteriol* 189:7663–7668.
22. Elfarash A, Wei Q, Cornelis P (2012) The soluble pyocins S2 and S4 from *Pseudomonas aeruginosa* bind to the same FpvAI receptor. *MicrobiologyOpen* 1:268–275.
23. Noinaj N, Guillier M, Barnard TJ, Buchanan SK (2010) TonB-dependent transporters: Regulation, structure, and function. *Annu Rev Microbiol* 64:43–60.
24. Greenwald J, et al. (2007) Real time fluorescent resonance energy transfer visualization of ferric pyoverdine uptake in *Pseudomonas aeruginosa*. A role for ferrous iron. *J Biol Chem* 282:2987–2995.
25. Adams H, Zeder-Lutz G, Schalk I, Pattus F, Celia H (2006) Interaction of TonB with the outer membrane receptor FpvA of *Pseudomonas aeruginosa*. *J Bacteriol* 188: 5752–5761.
26. Rassam P, et al. (2015) Supramolecular assemblies underpin turnover of outer membrane proteins in bacteria. *Nature* 523:333–336.
27. McCaughey LC, et al. (2016) Discovery, characterization and in vivo activity of pyocin SD2, a protein antibiotic from *Pseudomonas aeruginosa*. *Biochem J* 473:2345–2358.
28. Poole K, Zhao Q, Neshat S, Heinrichs DE, Dean CR (1996) The *Pseudomonas aeruginosa tonB* gene encodes a novel TonB protein. *Microbiology* 142:1449–1458.
29. Hilsenbeck JL, et al. (2004) Crystal structure of the cytotoxic bacterial protein colicin B at 2.5 A resolution. *Mol Microbiol* 51:711–720.
30. Mosbahi K, et al. (2002) The cytotoxic domain of colicin E9 is a channel-forming endonuclease. *Nat Struct Biol* 9:476–484.
31. Farrance OE, et al. (2013) A force-activated trip switch triggers rapid dissociation of a colicin from its immunity protein. *PLoS Biol* 11:e1001489.
32. Dietz H, Rief M (2004) Exploring the energy landscape of GFP by single-molecule mechanical experiments. *Proc Natl Acad Sci USA* 101:16192–16197.
33. Hickman SJ, Cooper REM, Bellucci L, Paci E, Brockwell DJ (2017) Gating of TonB-dependent transporters by substrate-specific forced remodelling. *Nat Commun* 8:14804.
34. Chimento DP, Mohanty AK, Kadner RJ, Wiener MC (2003) Substrate-induced transmembrane signaling in the cobalamin transporter BtuB. *Nat Struct Biol* 10:394–401.
35. Chimento DP, Kadner RJ, Wiener MC (2005) Comparative structural analysis of TonB-dependent outer membrane transporters: Implications for the transport cycle. *Proteins* 59:240–251.
36. Wallis R, Moore GR, James R, Kleanthous C (1995) Protein-protein interactions in colicin E9 DNase-immunity protein complexes. 1. Diffusion-controlled association and femtomolar binding for the cognate complex. *Biochemistry* 34:13743–13750.
37. Vankemmelbeke M, et al. (2009) Energy-dependent immunity protein release during *tol*-dependent nuclease colicin translocation. *J Biol Chem* 284:18932–18941.
38. Wiedemann N, Pfanner N (2017) Mitochondrial machineries for protein import and assembly. *Annu Rev Biochem* 86:685–714.
39. Taylor R, Burgner JW, Clifton J, Cramer WA (1998) Purification and characterization of monomeric *Escherichia coli* vitamin B12 receptor with high affinity for colicin E3. *J Biol Chem* 273:31113–31118.
40. Greenwald J, Zeder-Lutz G, Hagege A, Celia H, Pattus F (2008) The metal dependence of pyoverdine interactions with its outer membrane receptor FpvA. *J Bacteriol* 190: 6548–6558.
41. Shen J, Meldrum A, Poole K (2002) FpvA receptor involvement in pyoverdine biosynthesis in *Pseudomonas aeruginosa*. *J Bacteriol* 184:3268–3275.
42. Kabsch W (2010) Xds. *Acta Crystallogr D Biol Crystallogr* 66:125–132.
43. Evans PR, Murshudov GN (2013) How good are my data and what is the resolution? *Acta Crystallogr D Biol Crystallogr* 69:1204–1214.
44. Winn MD, et al. (2011) Overview of the CCP4 suite and current developments. *Acta Crystallogr D Biol Crystallogr* 67:235–242.
45. McCoy AJ, et al. (2007) Phaser crystallographic software. *J Appl Cryst* 40:658–674.
46. Greenwald J, et al. (2009) FpvA bound to non-cognate pyoverdines: Molecular basis of siderophore recognition by an iron transporter. *Mol Microbiol* 72:1246–1259.
47. Adams PD, et al. (2010) PHENIX: A comprehensive Python-based system for macromolecular structure solution. *Acta Crystallogr D Biol Crystallogr* 66:213–221.
48. Bricogne GBE, et al. (2010) BUSTER (Global Phasing Ltd, Cambridge, United Kingdom), Version 2.10.2.
49. Emsley P, Cowtan K (2004) Coot: Model-building tools for molecular graphics. *Acta Crystallogr D Biol Crystallogr* 60:2126–2132.
50. Chen VB, et al. (2010) MolProbity: All-atom structure validation for macromolecular crystallography. *Acta Crystallogr D Biol Crystallogr* 66:12–21.
51. Krissinel E, Henrick K (2007) Inference of macromolecular assemblies from crystalline state. *J Mol Biol* 372:774–797.
52. Delano WL (2002) *The PyMOL Molecular Graphics System* (DeLano Scientific, Palo Alto, CA).
53. Chin JW, Martin AB, King DS, Wang L, Schultz PG (2002) Addition of a photocrosslinking amino acid to the genetic code of *Escherichiacoli*. *Proc Natl Acad Sci USA* 99:11020–11024.
54. Marino F, et al. (2014) Characterization and usage of the EASY-spray technology as part of an online 2D SCX-RP ultra-high pressure system. *Analyst (Lond)* 139: 6520–6528.
55. Yang B, et al. (2012) Identification of cross-linked peptides from complex samples. *Nat Methods* 9:904–906.
56. Schanda P, Kupče E, Brutscher B (2005) SOFAST-HMQC experiments for recording two-dimensional heteronuclear correlation spectra of proteins within a few seconds. *J Biomol NMR* 33:199–211.
57. Braunschweiler L, Ernst RR (1983) Coherence transfer by isotropic mixing–Application to proton correlation spectroscopy. *J Magn Reson* 53:521–528.
58. Delaglio F, et al. (1995) NMRPipe: A multidimensional spectral processing system based on UNIX pipes. *J Biomol NMR* 6:277–293.
59. Vranken WF, et al. (2005) The CCPN data model for NMR spectroscopy: Development of a software pipeline. *Proteins* 59:687–696.